Available online at www.sciencedirect.com
SCIENCE DIRECT®
Journal of Computational Physics 208 (2005) 469–492
JOURNAL OF COMPUTATIONAL PHYSICS
www.elsevier.com/locate/jcp

A Perfectly Matched Layer absorbing boundary condition for linearized Euler equations with a non-uniform mean flow

Fang Q. Hu *

Department of Mathematics and Statistics, Old Dominion University, Norfolk, VA 23529, United States

Received 3 August 2004; received in revised form 1 February 2005; accepted 13 February 2005
Available online 4 May 2005

Abstract

A Perfectly Matched Layer (PML) for linearized Euler equations with a parallel non-uniform mean flow is presented. The PML is formulated by utilizing a proper space–time transformation in its derivation so that in the transformed coordinates all dispersive waves supported by the non-uniform flow have consistent phase and group velocities. The space–time transformation is determined through a study of dispersion relations of all the linear waves. The proposed PML equations are applicable to both bounded and unbounded flows and given in unsplit physical variables. Furthermore, the stability of the PML is also considered. It is shown that the proposed PML is stable for a finite range of the absorption coefficient. Numerical examples that demonstrate the validity and effectiveness of PML as an absorbing boundary condition are presented.

Keywords: Non-reflecting boundary condition; Perfectly Matched Layer; Euler equations; Computational acoustics

1. Introduction

Non-reflecting boundary condition is necessary in all finite element and finite difference computations that involve wave propagation to open or semi-open physical domains. It remains a significant challenge particularly for fluids related problems where the governing equations are non-linear or have non-constant coefficients. The need for accurate non-reflecting boundary condition has become even greater after the substantial progresses made in recent years in the discretization methods, such as the utilization of high-order schemes and unstructured meshes as well as orders-of-magnitude improvement in high performance

* Tel.: +1 804 683 3882; fax: +1 804 683 3885.
E-mail address: fhu@odu.edu.

0021-9991/$ - see front matter © 2005 Elsevier Inc. All rights reserved.
doi:10.1016/j.jcp.2005.02.028

computing power. Non-reflecting boundaries are often the sources of most significant numerical errors in many practical computations.

In this paper, we develop non-reflecting boundary condition for the linearized Euler equations with a parallel non-uniform mean flow based on the Perfectly Matched Layer (PML) methodology. PML was originally developed as an absorbing boundary condition for computational electro-magnetics [6,11,33,26,9,31]. The significance of the PML technique lies in the fact that, for multi-dimensional problems, the absorbing zone so constructed can be theoretically reflectionless for out-going waves of any angle and frequency. However, early works on the extension of PML technique to the Euler equations in fluid dynamics indicated that a direct adaptation of the original split formulation could lead to numerical instability problems [16,17,1,27].

Substantial progresses have been made in recent studies regarding the PML for fluids dynamics [27,18,5,3,13]. It has now been recognized that the cause for instability in previous PML formulations is that the Euler equations, with a convective mean flow, support waves with phase and group velocities in opposite directions and these waves are actually amplified and become instability waves under the original PML formulation [18]. Consequently, a necessary condition for any wave to be absorbed, and not amplified, under the original PML technique is that its phase and group velocities must be consistent. Recognizing this, new formulations of PML have appeared in the literature [18,12,13,3]. For instance, in [18], a stable PML for the linearized Euler equations with a *uniform* mean flow was proposed. It employed a space–time transformation before applying the PML technique so that in the transformed coordinates all waves have consistent phase and group velocities. This has led to a dynamically stable and highly effective absorbing boundary condition. The method used in [18] has also been recently applied to the shallow water equation in geophysics [2].

The focus of this paper is on the formulation of stable PML for Euler equations with *non-uniform* mean flows. Recently, in [13], a formulation of PML for linearized Euler equations with a uniform mean flow was extended to non-uniform flows, in which one parameter of the layer was adjusted numerically to maintain stability. The main issue, as we will show in this paper, is how to choose a priori the proper space–time transformation when the mean flow is non-uniform so that all waves supported by the governing equations have consistent phase and group velocities in the transformed coordinates. It will be shown in the current work that such a space–time transformation can be determined based on the study of *dispersive waves* of the Euler equations. By an application of the proper space–time transformation, stable PML equations can be constructed following the technique used in [18]. The emphasis of the paper will be on how to extend the technique used in [18] to the case of non-uniform mean flows. The effectiveness of the approach will be demonstrated through numerical examples.

The rest of the paper is organized as follows. In the next section, recent progresses are reviewed and the importance of understanding the dispersion relations of linear waves for the construction of stable PML is discussed. Then, a detailed study on all dispersive waves supported by the Euler equations with a wall bounded non-uniform mean flow is presented in Section 3. Following a proper space–time transformation suggested by the study in Section 3, the derivation of PML equation is given in Section 4. In Section 5, the stability of proposed PML equation is studied. The PML for unbounded flows are presented in Section 6. Finally, numerical examples are reported in Section 7 that demonstrate the validity and efficiency of the PML as an absorbing boundary condition. Section 8 contains concluding remarks.

2. Dispersive waves and the stability of PML

In this section, a brief review of recent works on PML for the Euler equations (see, e.g., [1,5,3,12,13,18,27]) will be given, which emphasizes the importance of understanding the dispersive waves of the physical system in constructing stable PMLs.

One view of the PML technique is that it is a complex change of variable in the frequency domain [7,9,11,26,31] and this view will be assumed in the present investigation. For simplicity, all discussions in this section will be limited to the construction of a vertical x-layer which involves a PML complex change of variable for x as

$$x \to x + \frac{\mathrm{i}}{\omega} \int_{x_0}^{x} \sigma_x \, \mathrm{d}x, \tag{1}$$

where $\sigma_x > 0$ is the absorption coefficient (a constant or a function of x) and x_0 is the location of the PML/Euler interface. Other alternative forms of (1) are possible, such as the one given in [4] for long time stability, but they will not alter the basic arguments provided below. As a heuristic argument, consider a wave ansatz of the form

$$\mathrm{e}^{\mathrm{i}(kx-\omega t)}. \tag{2}$$

Under the complex change of variable (1), it becomes

$$\mathrm{e}^{\mathrm{i}(kx-\omega t)} \mathrm{e}^{-\frac{k}{\omega}\int_{x_0}^{x} \sigma_x \mathrm{d}x}. \tag{3}$$

The second factor in expression (3) indicates that the wave amplitude decays exponentially in the PML zone if and only if

$$\frac{k}{\omega} \int_{x'}^{x} \sigma_x \, \mathrm{d}x > 0 \tag{4}$$

as the wave propagates from an arbitrary location x' in the PML zone. This means that the PML is only absorbing for a wave that *propagates to the right (x increasing) with $k/\omega > 0$* or *propagates to the left (x decreasing) with $k/\omega < 0$*. In other words, for the amplitude of the wave to be reducing (and not increasing) in the PML domain, the direction of wave propagation should be consistent with the sign of k/ω or, equivalently, the phase velocity ω/k [18,5]. Since the direction of propagation of a dispersive wave is determined by the group velocity, this necessary condition has been expressed nicely in [5] as

$$\frac{k}{\omega} \frac{\mathrm{d}\omega}{\mathrm{d}k} > 0, \tag{5}$$

or, equivalently,

$$c_{\mathrm{ph}} c_{\mathrm{g}} > 0 \tag{6}$$

where c_{ph} and c_{g} are, respectively, the phase velocity, ω/k, and the group velocity, $\mathrm{d}\omega/\mathrm{d}k$. That is, for the PML technique to yield stable absorbing boundary conditions, the phase and group velocities of the physical waves must be consistent and in the same direction. Conversely, any wave of the original physical system having its phase and group velocities in opposite directions will be exponentially amplified and result in instability in the PML domain. Condition (5) links intimately the construction of stable PMLs to the dispersion relation, i.e., $\omega = \omega(k)$, of the physical waves under investigation.

This necessary condition for stable PML has been recognized in several recent studies [27,18,5,13]. For instance, in [18], it was pointed out that, in the presence of a convective mean flow, the Euler equations support acoustic waves that have *a positive group velocity but a negative phase velocity* and these waves were actually amplified in previous PML formulations. It was further proposed in [18] that, when deriving the PML equation for the Euler equations, a proper space–time transformation be used before applying the PML technique so that in the transformed coordinates all linear waves supported by the Euler equations have consistent phase and group velocities. For the linearized Euler equations with a *uniform* mean flow in the x-direction, the proper space–time transform involved essentially a transformation in time of the form

$$\bar{t} = t + \beta x, \tag{7}$$

where

$$\beta = \frac{\bar{U}_0}{1 - \bar{U}_0^2} \tag{8}$$

in which $\bar{U}_0$ is the *uniform* mean flow Mach number [18]. The corresponding transformation in the frequency–wavenumber space is

$$\bar{k} = k + \beta\omega, \quad \bar{\omega} = \omega. \tag{9}$$

The value of β in (8) was determined so that the dispersion relation of the convective acoustic waves, namely,

$$(\omega - \bar{U}_0 k)^2 - k^2 - k_y^2 = 0$$

becomes the following in the transformed space

$$\bar{\omega}^2/(1 - \bar{U}_0^2) - (1 - \bar{U}_0^2)\bar{k}^2 - k_y^2 = 0$$

for which the phase and group velocities are consistent [18]. This transformation is similar to the well-known "Prandtl–Glauert" transformation in aerodynamics. In [18], a new PML equation was formulated by applying the complex change of variable (1) in the transformed coordinates in the derivation process. It was demonstrated that the new PML formulation was dynamically stable and perfectly matched to the Euler equations for the acoustic, vorticity and entropy waves. The importance of the space–time transformation (7) and the particular choice for β in (8) were also confirmed in recent independent formulations in [3,12,13]. For example, in [13], the importance of the transformation (7) was reflected by forming a special wave ansatz. An extension of PML to non-uniform mean flows was also given in [13] where an equivalent value for β, called μ, was adjusted by numerical experiments that gave stable solutions.

The question becomes whether it is still possible to determine a priori the proper space–time transformation for the Euler equations with an arbitrary *non-uniform* mean flows so that, in the transformed coordinates, all linear waves have consistent phase and group velocities. We will show in the next section that, for a parallel non-uniform mean flow, it is again possible, and necessary, to apply a transformation of the form (7) in the derivation of PML equation and the value for β in (7), actually a unique choice, can be determined through a study of the dispersion relations of the physical waves.

3. Linear waves of Euler equations with a non-uniform mean flow bounded by solid walls

Let the linearized Euler equations with a parallel non-uniform mean flow be written as

$$\frac{\partial \mathbf{u}}{\partial t} + \mathbf{A}\frac{\partial \mathbf{u}}{\partial x} + \mathbf{B}\frac{\partial \mathbf{u}}{\partial y} + \mathbf{C}\mathbf{u} = 0 \tag{10}$$

in which

$$\mathbf{u} = \begin{pmatrix} \rho \\ u \\ v \\ p \end{pmatrix}, \quad \mathbf{A} = \begin{pmatrix} \bar{U} & \bar{\rho} & 0 & 0 \\ 0 & \bar{U} & 0 & \frac{1}{\bar{\rho}} \\ 0 & 0 & \bar{U} & 0 \\ 0 & 1 & 0 & \bar{U} \end{pmatrix}, \quad \mathbf{B} = \begin{pmatrix} 0 & 0 & \bar{\rho} & 0 \\ 0 & 0 & 0 & 0 \\ 0 & 0 & 0 & \frac{1}{\bar{\rho}} \\ 0 & 0 & 1 & 0 \end{pmatrix}, \quad \mathbf{C} = \begin{pmatrix} 0 & 0 & \frac{\mathrm{d}\bar{\rho}}{\mathrm{d}y} & 0 \\ 0 & 0 & \frac{\mathrm{d}\bar{U}}{\mathrm{d}y} & 0 \\ 0 & 0 & 0 & 0 \\ 0 & 0 & 0 & 0 \end{pmatrix},$$

where u and v are velocity components in the x and y directions respectively, non-dimensionalized by a reference speed of sound a_0; ρ is the density, non-dimensionalized by a reference value ρ_0; and p is the pressure, non-dimensionalized by $\rho_0 a_0^2$. Also, the space variables x and y are non-dimensionalized by a reference scale ℓ_0 and time t is non-dimensionalized by ℓ_0/a_0. The mean velocity $\bar{U}(y)$ and density $\bar{\rho}(y)$ are functions of y only and the mean pressure is constant. We note that, alternatively, Eq. (10) can be formed by a $\mathbf{u}$ vector that contains only u, v and p, since the equation for density ρ can be separated. This will result in a smaller system, but will not affect our derivation of the PML equation.

As the discussion in the previous section shows, the construction of stable PML depends on the dispersion relations of the physical waves supported by the Euler equations. In this section, we conduct a study of linear waves of (10) in a parallel flow bounded by solid walls at $y = \pm 1$, as shown in Fig. 1. For this purpose, a linear wave analysis for (10) will be carried out numerically, since a closed form dispersion relation is not available for non-uniform mean flows. In this approach, we seek solutions to (10) of the form

$$\mathbf{u}(x,y,t) = \hat{\mathbf{u}}(y)\mathrm{e}^{\mathrm{i}(kx-\omega t)}, \tag{11}$$

where ω and k are the frequency and wavenumber respectively. By substituting (11) into the Euler equation (10), we get an eigenvalue problem

$$-\mathrm{i}\omega\hat{\mathbf{u}} + \mathrm{i}k\mathbf{A}\hat{\mathbf{u}} + \mathbf{B}\frac{\mathrm{d}\hat{\mathbf{u}}}{\mathrm{d}y} + \mathbf{C}\hat{\mathbf{u}} = 0 \tag{12}$$

with these homogeneous boundary conditions,

$$\frac{\mathrm{d}\hat{u}}{\mathrm{d}y} = \hat{v} = \frac{\mathrm{d}\hat{p}}{\mathrm{d}y} = \frac{\mathrm{d}\hat{\rho}}{\mathrm{d}y} = 0 \quad \text{at } y = \pm 1. \tag{13}$$

This eigenvalue problem will be solved by a spectral collocation method which is a standard method in hydrodynamic stability analysis [25,10,22]. Further details are given in Appendix A. It yields a complete spectrum of all normal modes supported by (12). Each eigenvalue ω of (12) as a function of given wavenumber k defines the dispersion relation $\omega = \omega(k)$ for that wave mode.

As a specific example, we will demonstrate the dispersion relations of all linear waves associated with a shear flow of mean velocity

$$\bar{U}(y) = \frac{1}{2}\left[(U_1 + U_2) + (U_1 - U_2)\tanh\left(\frac{2y}{\delta}\right)\right] \tag{14}$$

and mean density

$$\bar{\rho}(y) = \frac{1}{\bar{T}(y)} \tag{15}$$

with

$$\bar{T}(y) = T_1\frac{\bar{U} - U_2}{U_1 - U_2} + T_2\frac{U_1 - \bar{U}}{U_1 - U_2} + \frac{\gamma - 1}{2}(U_1 - \bar{U})(\bar{U} - U_2),$$

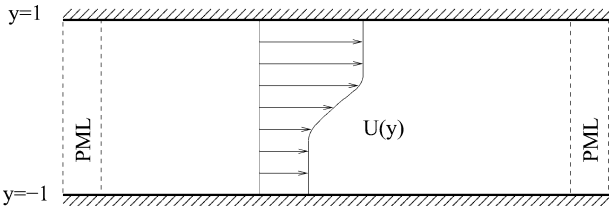

Fig. 1. A schematic of a bounded parallel non-uniform mean flow.

where the mean temperature $\bar{T}(y)$ is determined by the Crocco relation for compressible flows. $\gamma = 1.4$. The mean flow parameters chosen for the example are as follows:

$$U_1 = 0.8, \quad U_2 = 0.2, \quad \delta = 0.4, \quad T_1 = 1, \quad T_2 = 0.8.$$

The mean velocity and density profiles are plotted in Fig. 2. Both are non-constant.

Fig. 3 shows the dispersion relations diagram of all the normal modes of (12), i.e., ω_r (real part of ω) vs. k. The imaginary part is zero for all wave modes except the Kelvin–Helmholtz instability wave which will be shown later.

In the dispersion relations diagram, we see two families of waves. One family has phase speed between $U_{min} = 0.2$ and $U_{max} = 0.8$, shown between dashed lines in Fig. 3. They are actually a discretization of a continuous spectrum. For convenience of discussion, these waves will be referred to as "vortical" modes in this paper. The vortical modes convect with the mean flow. We see that for the vortical modes, both the group and phase velocities are positive. Therefore condition (5) is satisfied. We note that one of the vortical modes is the Kelvin–Helmholtz instability wave supported by the present mean flow profile. An enlarged graph is shown in Fig. 4 for the real and imaginary parts of ω as functions of k where the Kelvin–Helmholtz wave, as well as its complex conjugate, is highlighted by circles.

The other family of waves in the dispersion relation diagram in Fig. 3 will be referred to as "acoustic" modes. A closer examination on the phase speed of the acoustic modes will show that they always have a phase speed supersonic relative to part of the mean flow. Furthermore, they are *dispersive waves* [32], where

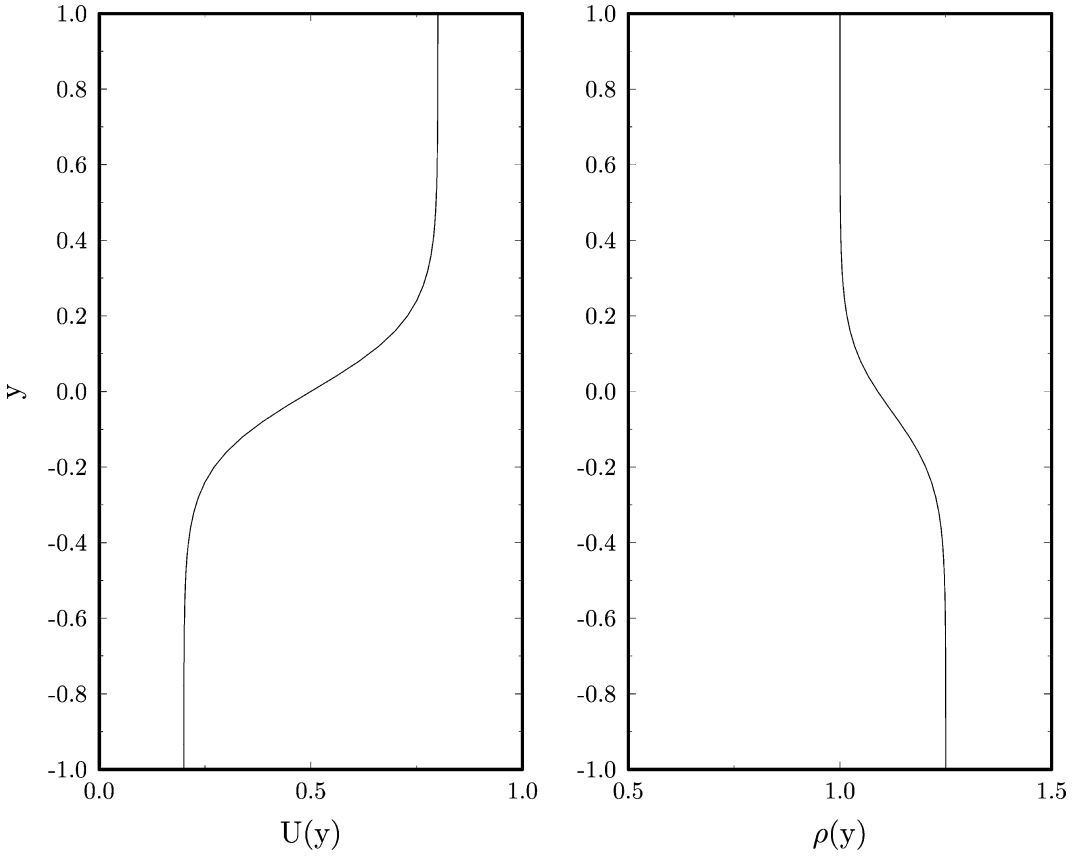

Fig. 2. Mean velocity and density used in the example.

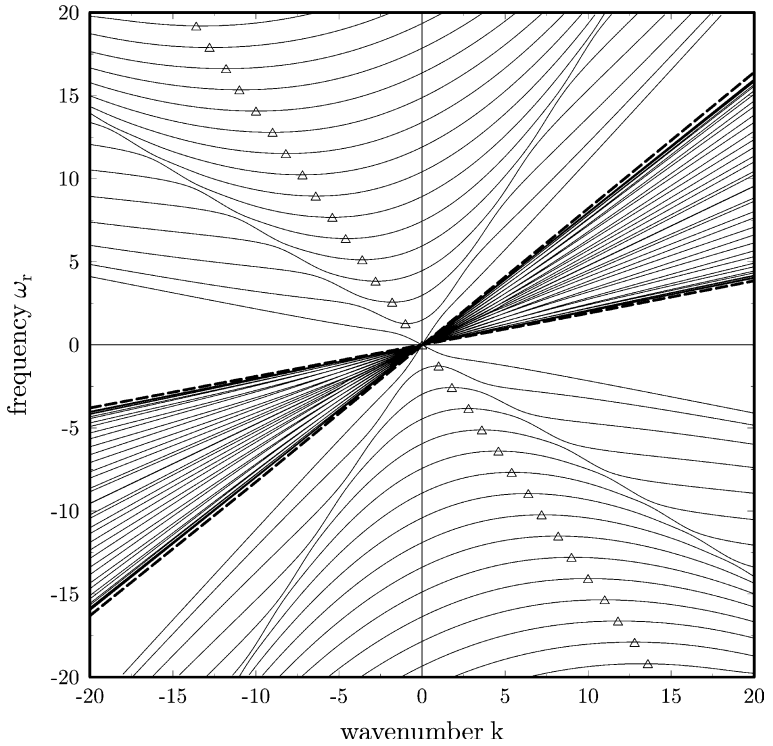

Fig. 3. Dispersion relation diagram. Triangles denote the points of zero group velocity. Dashed lines are $\omega_r = U_1 k$ and $\omega_r = U_2 k$.

$\omega/k \neq$ constant. Fig. 3 also shows that the acoustic modes do not always have consistent phase and group velocities. A triangle on the acoustic waves indicates the location where the group velocity is zero, i.e., $d\omega_r/dk = 0$. As we can see, for the acoustic modes in the upper left and lower right quarters in Fig. 3 that lie between the triangle and the vertical axis, their phase velocity (ω_r/k) is negative but their group velocity ($d\omega_r/dk$) is positive. By the argument provided in the previous section, applying directly the PML complex change of variable (1) to the Euler equation (10) without a proper space–time coordinate transformation in the derivation process will result in these waves being amplified and becoming unstable waves.

To find the proper space–time transformation, we note that, remarkably, the locations of zero group velocity points on the dispersion diagram (triangles in Fig. 3) appear to lie closely on a straight line. This implies that a linear space–time transformation of the form (7), which incurs a transformation in the frequency–wavenumber space of the form (9), can again be used to "correct" the dispersion relation. The obvious choice for β in (7) and (9) is

$$\beta = -\frac{1}{c_0}, \tag{16}$$

where c_0 is the slope of the line of triangles ($\omega_r = c_0 k$) in Fig. 3. In Table 1, the locations of the zero group velocity points for the first 20 acoustic modes are listed. For the current example, Table 1 suggests a value $c_0 \approx -1.4073$.

The dispersion relation diagram in the transformed coordinates is shown in Fig. 5. Now all the waves have approximately consistent phase and group velocities and, therefore, satisfy condition (5).

It is important to point out that it does not appear to be accidental that all points of zero group velocity fall closely on a straight line. For other types of subsonic mean flow profiles, including mixing layers, jets, wakes, as well as viscous boundary layer flows, it was found, at least numerically, that the points of zero

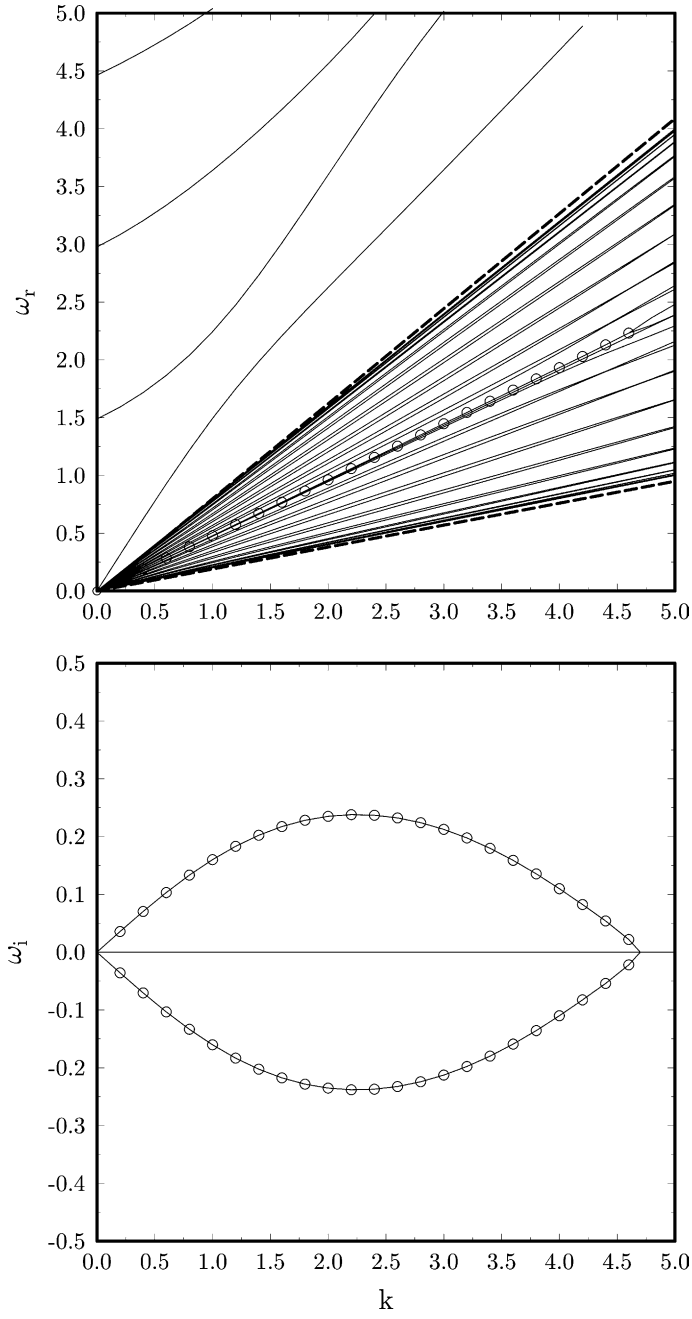

Fig. 4. Dispersion relation diagram enlarged from Fig. 3. Top: ω_r (real part of ω) vs. k; bottom: ω_i (imaginary part of ω) vs. k. The circles highlight the Kelvin–Helmholtz instability wave.

group velocity on the dispersion diagram for the acoustic modes were always closely lined. Two further examples of jet and plane Poiseuille flows are shown in Fig. 6. It is also worth pointing out that if part of the mean flow is supersonic, it has been found that each acoustic mode will have two locations where

Table 1
Values of k_0 and ω_0 where the group velocity is zero in Fig. 3

Mode number	k_0	ω_0	ω_0/k_0
1	±0.09291	∓1.2721	−1.3692
2	±1.7852	∓2.5675	−1.4382
3	±2.7414	∓3.8293	−1.3969
4	±3.6331	∓5.1200	−1.4091
5	±4.5378	∓6.3924	−1.4086
6	±5.4594	∓7.6739	−1.4056
7	±6.3559	∓8.9519	−1.4084
8	±7.2725	∓10.2308	−1.4068
9	±8.1773	∓11.5097	−1.4075
10	±9.0874	∓12.7885	−1.4072
11	±10.9045	∓15.3462	−1.4073
12	±11.8134	∓16.6250	−1.4073
13	±12.7220	∓17.9038	−1.4073
14	±13.6308	∓19.1827	−1.4073
15	±14.5394	∓20.4615	−1.4073
16	±15.4482	∓21.7403	−1.4073
17	±16.3569	∓23.0192	−1.4073
18	±17.2656	∓24.2980	−1.4073
19	±18.1743	∓25.5769	−1.4073
20	±19.0830	∓26.8557	−1.4073

the group velocity becomes zero [20], which would make the linear transformation (7) alone ineffective for transonic mean flows.

4. Derivation of PML equations

4.1. Unsplit formulation

Once the value of β for the proper space–time transformation (7) has been determined based on the dispersion relations of the acoustic modes, the derivation of PML for the Euler equations can be carried out as follows. We shall first apply the space–time transformation (7) to the governing equations so that all dispersive waves have consistent phase and group velocities. Then, the PML complex change of variable (1) will be applied in the transformed coordinates. And finally the PML equation in the original physical time domain is obtained. Details are given below.

Under transformation (7), we have these changes in the partial derivatives

$$\frac{\partial}{\partial t} \to \frac{\partial}{\partial \bar{t}}, \quad \frac{\partial}{\partial x} \to \frac{\partial}{\partial x} + \beta \frac{\partial}{\partial \bar{t}}, \tag{17}$$

and the Euler equation (10) in transformed coordinates becomes

$$(\mathbf{I} + \beta \mathbf{A}) \frac{\partial \mathbf{u}}{\partial \bar{t}} + \mathbf{A} \frac{\partial \mathbf{u}}{\partial x} + \mathbf{B} \frac{\partial \mathbf{u}}{\partial y} + \mathbf{C}\mathbf{u} = 0. \tag{18}$$

The PML technique will first be applied to the transformed equation (18). As in [18], we first write (18) in the frequency domain,

$$-\mathrm{i}\bar{\omega}(\mathbf{I} + \beta \mathbf{A})\tilde{\mathbf{u}} + \mathbf{A} \frac{\partial \tilde{\mathbf{u}}}{\partial x} + \mathbf{B} \frac{\partial \tilde{\mathbf{u}}}{\partial y} + \mathbf{C}\tilde{\mathbf{u}} = 0, \tag{19}$$

in which $\mathbf{u}(x, y, \bar{t}) = \tilde{\mathbf{u}}(x, y)\mathrm{e}^{-\mathrm{i}\bar{\omega}\bar{t}}$ is assumed.

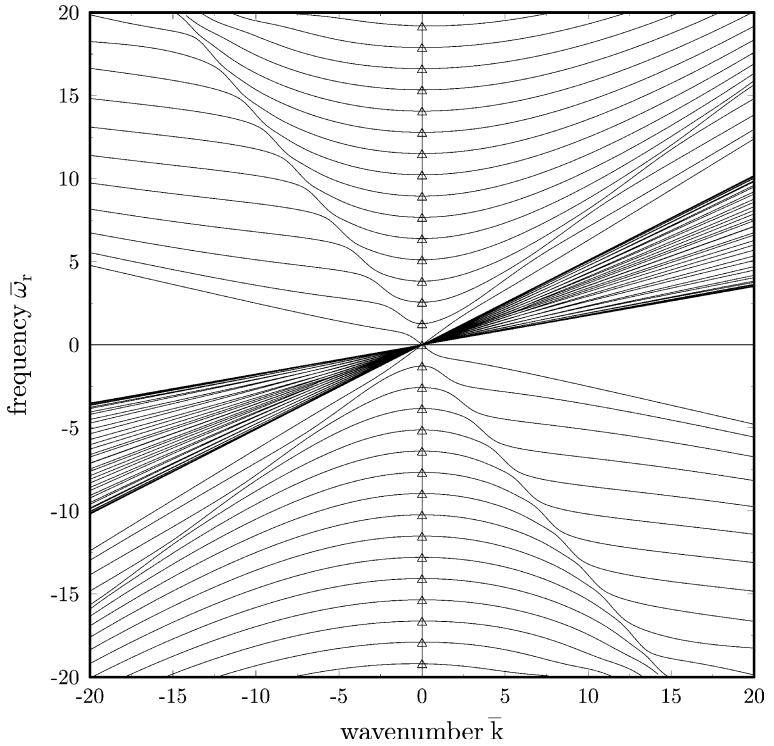

Fig. 5. Dispersion relation diagram in transformed space. Triangles denote the points of zero group velocity.

To construct the PML equation for the vertical x-layer, we apply the PML complex change of variable (1) to the frequency domain equation (19) which involves a change in the partial derivative with respect to x as

$$\frac{\partial}{\partial x} \to \frac{1}{1+\frac{i\sigma_x}{\omega}} \frac{\partial}{\partial x}, \tag{20}$$

where σ_x is a positive function of x. That is, Eq. (19) is modified to be

$$-i\bar{\omega}(\mathbf{I}+\beta\mathbf{A})\tilde{\mathbf{u}} + \frac{1}{1+\frac{i\sigma_x}{\bar{\omega}}}\mathbf{A}\frac{\partial \tilde{\mathbf{u}}}{\partial x} + \mathbf{B}\frac{\partial \tilde{\mathbf{u}}}{\partial y} + \mathbf{C}\tilde{\mathbf{u}} = 0. \tag{21}$$

Eq. (21) is the PML equation for the x-layer in the frequency domain. It will now be written back in the time domain by following an unsplit approach used in [7,11,18,31]. By multiplying the equation with $1+\frac{i\sigma_x}{\bar{\omega}}$, we get

$$(-i\bar{\omega}+\sigma_x)(\mathbf{I}+\beta\mathbf{A})\hat{\mathbf{u}} + \mathbf{A}\frac{\partial \hat{\mathbf{u}}}{\partial x} + \left(1+\frac{i\sigma_x}{\bar{\omega}}\right)\mathbf{B}\frac{\partial \hat{\mathbf{u}}}{\partial y} + \left(1+\frac{i\sigma_x}{\bar{\omega}}\right)\mathbf{C}\hat{\mathbf{u}} = 0.$$

Then the equivalent time domain equation for the above is easily found to be

$$(\mathbf{I}+\beta\mathbf{A})\left(\frac{\partial \mathbf{u}}{\partial \bar{t}} + \sigma_x \mathbf{u}\right) + \mathbf{A}\frac{\partial \mathbf{u}}{\partial x} + \mathbf{B}\left(\frac{\partial \mathbf{u}}{\partial y} + \sigma_x \frac{\partial \mathbf{q}}{\partial y}\right) + \mathbf{C}(\mathbf{u}+\sigma_x \mathbf{q}) = 0, \tag{22}$$

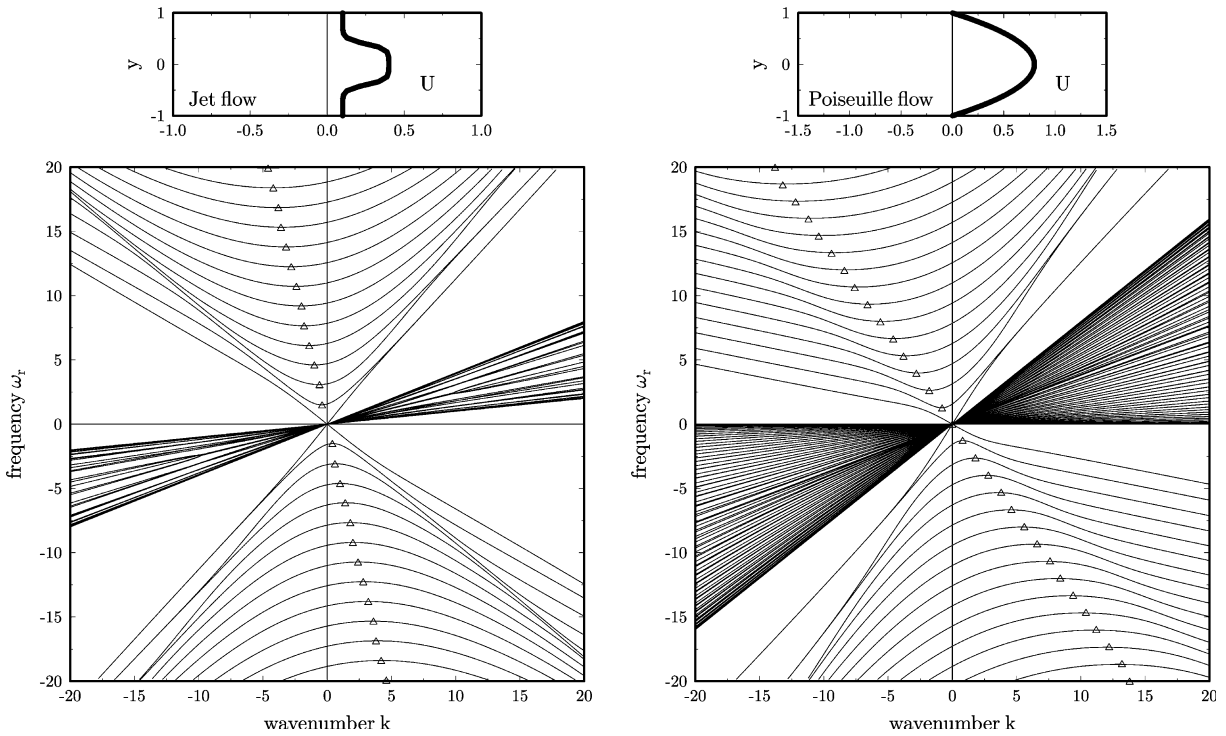

Fig. 6. Dispersion relation diagram of a jet (left) and a channel Poiseuille flow (right). Triangles denote the points of zero group velocity.

where $\mathbf{q}$ is an auxiliary variable defined as

$$\frac{\partial \mathbf{q}}{\partial t} = \mathbf{u}. \tag{23}$$

Finally, when (22) is written in the original physical coordinates (x, y, t), we get the following PML equation for (10) with non-uniform mean flows,

$$\frac{\partial \mathbf{u}}{\partial t} + \mathbf{A}\frac{\partial \mathbf{u}}{\partial x} + \mathbf{B}\left(\frac{\partial \mathbf{u}}{\partial y} + \sigma_x \frac{\partial \mathbf{q}}{\partial y}\right) + \mathbf{C}(\mathbf{u} + \sigma_x \mathbf{q}) + \sigma_x \mathbf{u} + \sigma_x \beta \mathbf{A}\mathbf{u} = 0, \tag{24}$$

where the equation for $\mathbf{q}$ is that given in (23). We note that $\mathbf{q}$ is only necessary inside the PML domains [18].

4.2. Absorption of hydrodynamic instability waves

It is well known that Euler equations can support hydrodynamic instability waves, for example, the Kelvin–Helmholtz instability for jets and mixing layers where the mean velocity profile has an inflection point. The PML should be absorbing to all waves, including the instability and evanescent waves. There are generally two kinds of hydrodynamic instabilities, namely the absolute and convective instabilities [23]. For numerical simulations, we are mostly concerned with the convective instability waves that grow spatially and propagate with the mean flow to the outflow boundary. A simple argument on the phase and group velocities, given below, will show that the PML formulated here will always absorb convective instability waves.

Suppose that the mean flow is from left to right. Then the group velocity of a convective instability wave that propagates with the mean flow will be positive, i.e.,

$$\frac{\mathrm{d}\omega_r}{\mathrm{d}k} > 0.$$

Furthermore, by an extension of the semi-circle theorem (in the theory of hydrodynamic stability) to compressible flows, it has been shown in [8] that the phase speed of any instability wave is bounded by the maximum and minimum values of the mean velocity, i.e.,

$$0 < U_{\min} \leqslant \frac{\omega_{\mathrm{r}}}{k} \leqslant U_{\max}. \tag{25}$$

Therefore, the phase and group velocities of a convective instability wave are both positive and condition (5) is always satisfied. This means that the spatial growth rate of convective instability waves will always be reduced in the PML zone. To completely annihilate the instability waves, the PML absorption rate should be designed such that it is greater than the spatial growth rate of the instability waves.

4.3. Value for β

The parameter β in Eq. (24) is a critical number for ensuring the stability of the PML equation. In the previous section, the proper value for β, appeared in the space–time transformation (7) used in the derivation of PML, has been determined as the negative reciprocal of the phase velocity c_0 of the acoustic wave modes at which the group velocity is zero. In other words, if in general $D(\omega, k) = 0$ is the dispersion relation, then

$$c_0 = \frac{\omega_0}{k_0} \quad \text{and} \quad \beta = -\frac{1}{c_0}, \tag{26}$$

where ω_0 and k_0 are the roots to the coupled equations

$$\begin{cases} D(\omega_0, k_0) = 0, \\ \frac{\partial D}{\partial k}(\omega_0, k_0) = 0. \end{cases} \tag{27}$$

This is certainly the case for the uniform mean flow where the exact dispersion relation for the acoustic wave is known, as discussed in Section 2. For non-uniform shear flows, although the acoustic modes have been found and studied extensively in the past, for example for jets [28], shear layers [29,14,15], wakes [34] and boundary layers [24], an explicit and direct relationship between the phase speed c_0 define in (26) and an arbitrary mean flow profile has not been available. The spectral collocation method, its details given in Appendix A, provides a general way of determining the dispersion relations for an arbitrary mean flow, from which the value for c_0 and, thus, β can be extracted. A special case is worth mentioning. If the mean density is constant, i.e., the non-dimensionalized mean density $\bar{\rho}(y) = 1$, it has been found that a reasonably good empirical formula for β for practical purposes is

$$\beta = \frac{\bar{U}_m}{1 - \bar{U}_m^2}, \tag{28}$$

where $\bar{U}_m$ is the average mean velocity,

$$\bar{U}_m = \frac{1}{b-a}\int_a^b \bar{U}(y)\,\mathrm{d}y \tag{29}$$

for a domain in $y \in [a, b]$.

5. Stability of the PML equations

When the value of β in the PML equation (24) is determined based on the dispersion relations of linear waves as described earlier, all the physical waves of the Euler equations become absorbed in the PML domain, and their amplitudes are going to be reduced exponentially as they travel in the PML domain. However, with the introduction of the auxiliary variable $\mathbf{q}$, the order of partial differential equations has increased (doubled). As a result of this, the PML system of equations (24) and (23) now admits additional non-physical waves. It is important that these additional wave modes are not exponentially growing. In this section, we study this issue and carry out a stability analysis for Eqs. (24) and (23) when σ_x is held constant.

Following the similar approach used in the analysis of the Euler equation (10) in Section 3, we seek solutions to (24) and (23) of the form

$$\mathbf{u}(x,y,t) = \hat{\mathbf{u}}(y)\mathrm{e}^{\mathrm{i}(kx-\omega t)}, \tag{30}$$

$$\mathbf{q}(x,y,t) = \hat{\mathbf{q}}(y)\mathrm{e}^{\mathrm{i}(kx-\omega t)}. \tag{31}$$

By substituting the above into (24) and (23), we get

$$(-\mathrm{i}\omega)\hat{\mathbf{u}} + \mathrm{i}k\mathbf{A}\hat{\mathbf{u}} + \mathbf{B}\left(\frac{\mathrm{d}\hat{\mathbf{u}}}{\mathrm{d}y} + \sigma_x\frac{\mathrm{d}\hat{\mathbf{q}}}{\mathrm{d}y}\right) + \mathbf{C}(\hat{\mathbf{u}} + \sigma_x\hat{\mathbf{q}}) + \sigma_x\hat{\mathbf{u}} + \sigma_x\beta\mathbf{A}\hat{\mathbf{u}} = 0, \tag{32}$$

$$(-\mathrm{i}\omega)\hat{\mathbf{q}} = \hat{\mathbf{u}}. \tag{33}$$

With homogeneous boundary condition (13) for $\hat{\mathbf{u}}$ and similarly for $\hat{\mathbf{q}}$, (32) and (33) again form an eigenvalue problem and can be solved by the spectral collocation method (see Appendix A). For any given wavenumber k, an eigenvalue ω with a positive imaginary part would indicate an exponentially growing wave.

In Figs. 7(a), (b) and (c), we plot the imaginary part of all wave modes of (32) and (33) where the value of σ_x is taken to be a fixed constant 0.2, 2.0 and 10.0, respectively, for wavenumber k in the range of -20 to 20. The mean flow profile in this example is the same as that used for the example in Fig. 3. For cases (a) and (b), we see that all wave modes have the imaginary part of ω below zero, including the original Kelvin–Helmholtz wave, indicating that the PML equation is dynamically stable, at least within the range of k being considered. For case (c) where $\sigma_x = 10$, however, some wave modes have emerged with positive imaginary parts and thus become unstable at high wave numbers. These modes are originated from the non-physical waves. Fig. 7(c) indicates that the PML equations (23) and (24) could have exponentially growing solutions if the value of σ_x is taken to be too large. This has been found to be typical that the system of (23) and (24) is stable when the value of the absorption coefficient is below certain limit, let which be denoted by σ_s, but admits unstable wave modes when σ_x is greater than that limiting value σ_s. Experiments show that the limiting value σ_s varies widely depending on the particular mean flow profile. For the current example, the limiting value $\sigma_s = 3$. For other mean flow profiles, such as a linear shear mean velocity [20], the limiting value has been found to be as large as 100.

For cases where the value for σ_s is too small, the fact that the PML is stable only when $\sigma_x \leqslant \sigma_s$ could mean that a relatively large PML domain might be needed to achieve a desirable degree of wave absorption, because the effectiveness of a PML domain depends on the magnitude of the absorption coefficient as well as the total width of the absorbing zone [16,19]. For such cases, one practical remedy could be to use grid stretching in the PML domain, so that its effective width is increased without employing more grid points [26,33,19]. A grid stretching is equivalent to simply modifying the x derivative terms of the PML equation as

$$\frac{\partial}{\partial x} \to \frac{1}{\alpha(x)}\frac{\partial}{\partial x}, \tag{34}$$

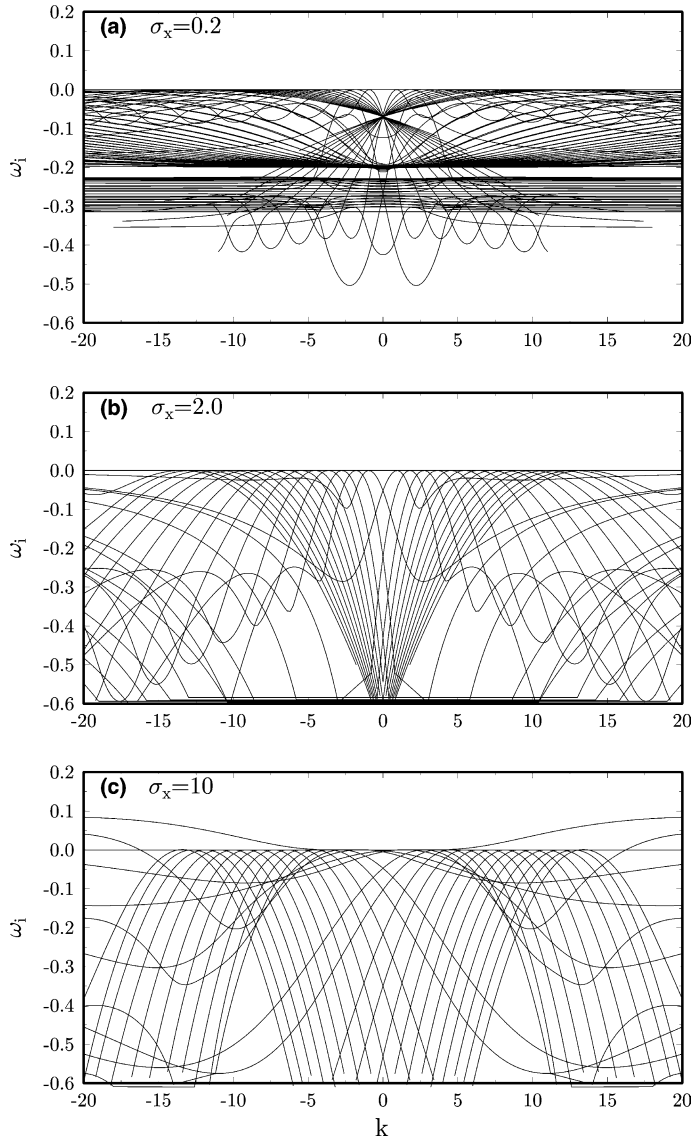

Fig. 7. Imaginary part of all wave modes: (a) $\sigma_x = 0.2$, (b) $\sigma_x = 2.0$, (c) $\sigma_x = 10.0$.

where $\alpha(x) \geqslant 1$ is a smooth function. For example,

$$\alpha(x) = 1 + A\left|\frac{x - x_0}{D}\right|^s, \tag{35}$$

where x_0 is the start of the PML domain and D its width. Grid stretching also has a side effect of introducing numerical damping which could improve the stability of PML even when σ_x is greater than the stability limiting value σ_s. This has been found to be quite effective in computations, as will be shown in the examples given later in Section 7.

6. PML for unbounded flows

When the flow is unbounded, horizontal y-layers are needed to terminate the computational domain at the top and bottom boundaries, as shown in Fig. 8. For a parallel mean flow aligned with the x-axis, the PML equation for the y-layers and corner layers can be developed by applying a complex change of variable in y, similar to (1) for x, namely,

$$y \to y + \int_{y_0}^{y} \sigma_y \, \mathrm{d}y \quad \text{and} \quad \frac{\partial}{\partial y} \to \frac{1}{1 + \frac{\mathrm{i}\sigma_y}{\omega}} \frac{\partial}{\partial y}, \tag{36}$$

to the frequency domain equation (21), where σ_y is a positive function of y. Upon rewriting the resulting equation in the time domain, we get a PML equation that is formally valid for all the vertical x-layers, horizontal y-layers as well as the corner layers. This is given below,

$$\frac{\partial \mathbf{u}}{\partial t} + \mathbf{A}\frac{\partial}{\partial x}(\mathbf{u} + \sigma_y \mathbf{q}) + \mathbf{B}\frac{\partial}{\partial y}(\mathbf{u} + \sigma_x \mathbf{q}) + \mathbf{C}(\mathbf{u} + \sigma_x \mathbf{q} + \sigma_y \mathbf{q} + \sigma_x \sigma_y \mathbf{q}') + (\sigma_x + \sigma_y)\mathbf{u} + \sigma_x \sigma_y \mathbf{q} + \sigma_x \beta \mathbf{A}(\mathbf{u} + \sigma_y \mathbf{q}) = 0, \tag{37}$$

where $\mathbf{q}'$ is another auxiliary variable defined as

$$\frac{\partial \mathbf{q}'}{\partial t} = \mathbf{q}.$$

While $\mathbf{q}'$ is only necessary at the corner layers (where both σ_x and σ_y are non-zero), we point out that in many practical applications the mean flow is uniform or nearly uniform within the y-layers, i.e., the we often have

$$\sigma_y \mathbf{C} \approx \mathbf{0}. \tag{38}$$

Therefore, the $\mathbf{q}'$ term can, in fact, be dropped from (37) for such cases. Equation (37) is perfectly matched to the Euler equation (10). We note that, except the term involving the $\mathbf{C}$ matrix, Eq. (37) is otherwise identical to the PML equation for a uniform mean flow given in [18], and it can be similarly made symmetrizable, thus strongly well-posed, by a slight modification as that given in [18]. Further implementation issues are referred to [18].

We note that even though the flow is now physically unbounded, it becomes bounded artificially due to the truncation of the computational domain in y, where solid wall like boundary conditions are usually applied at the end of the PML domains. To determine the value for β to be used for (37), a linear wave

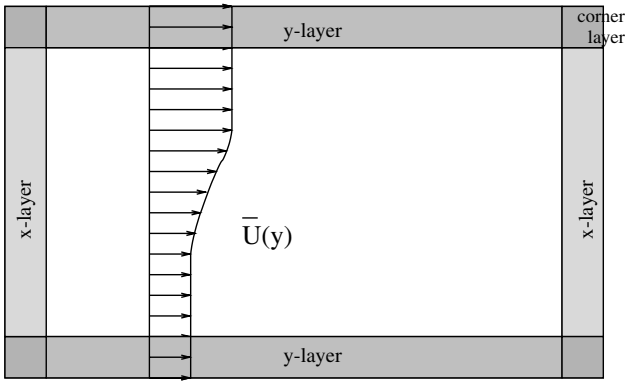

Fig. 8. A schematic of an unbounded parallel non-uniform mean flow, showing x-layers, y-layers and corner layers.

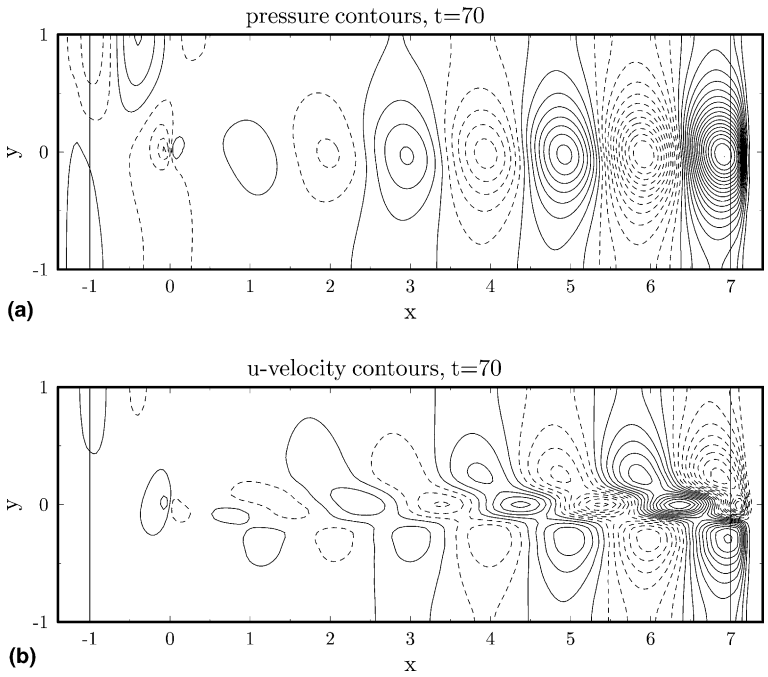

Fig. 9. Contours of the numerical solution at $t = 70$: (a) pressure, (b) u-velocity.

analysis similar to that of a wall bounded flow should now be carried out with the inclusion of the horizontal PML y-layers, namely, for the following equation:

$$\frac{\partial \mathbf{u}}{\partial t} + \mathbf{A}\frac{\partial}{\partial x}(\mathbf{u} + \sigma_y \mathbf{q}) + \mathbf{B}\frac{\partial \mathbf{u}}{\partial y} + \mathbf{C}(\mathbf{u} + \sigma_y \mathbf{q}) + \sigma_y \mathbf{u} = 0 \tag{39}$$

with appropriate homogeneous boundary conditions. Nonetheless, it was found that the presence of y-layers did not substantially alter the dispersion relations of the acoustic modes. Therefore, for simplicity, the value of β in (37) for unbounded flows could still be determined in the same way as that for the bounded flows described in previous sections, assuming that solid walls are placed at the top and bottom boundaries of the computational domain.

7. Numerical examples

In this section, three numerical examples will be presented, dealing with bounded and unbounded non-uniform mean flows. More examples can be found in [20].

7.1. Wall bounded shear flow

Consider a mixing layer, with the mean velocity and density specified by (14) and (15) and bounded by solid walls at $y = \pm 1$, as shown in Fig. 1. The Euler equation (10) with the following source term added to the equation of pressure:

$$s(x, y, t) = \sin(1.5t)\mathrm{e}^{-(\ln 2)(x^2+y^2)/0.05^2}, \tag{40}$$

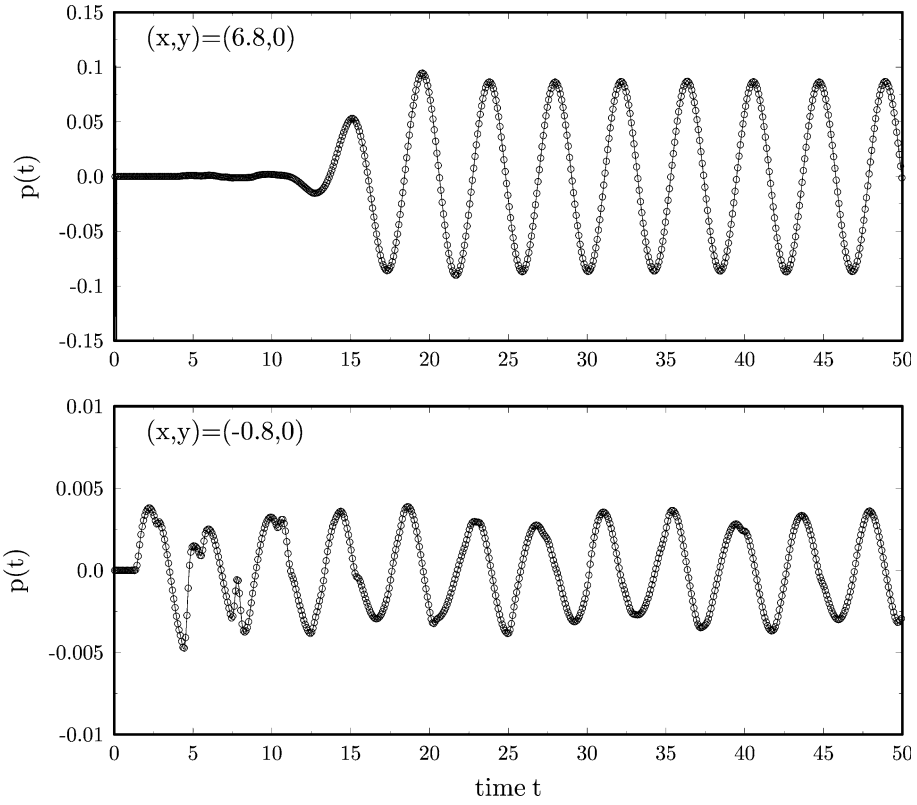

Fig. 10. Pressure time history. Solid line: numerical solution; circles: reference solution.

is solved by a finite difference scheme. For the results shown in Figs. 9–11, the computational domain is $[-1.4, 7.4]\times[-1, 1]$ with a uniform grid $\Delta x = \Delta y = 0.04$. Two PML domains, each consisting of 10 grid points, are used at the inflow and outflow boundaries. The absorption coefficient σ_x varies with x as

$$\sigma_x = \sigma_{\max}\left|\frac{x - x_0}{D}\right|^2, \tag{41}$$

where $\sigma_{\max} = 20$ and $x_0 = -1$ for the inflow and $x_0 = 7$ for the outflow PML domains. For the calculations reported here, a grid stretching of the form given in (35) is also used with the parameters being $A = 2$ and $s = 2$. All spatial derivatives are discretized by a 7-point DRP fourth-order central difference scheme [30], with a 10th-order filter applied throughout the computational domain [17]. Time integration is carried out by the optimized 5 and 6 stages alternating Low Dissipation and Low Dispersion Runge–Kutta scheme (LDDRK56) [21].

The added source term (40) generates an acoustic wave that is reflected repeatedly by the solid walls. At the same time, it excites the Kelvin–Helmholtz instability wave of the mixing layer that propagates downstream. Figs. 9(a) and (b) show the pressure and u-velocity contours, respectively, at time $t = 70$. Clearly, wave absorptions at both the inflow and outflow PML domains are quite effective.

In Fig. 10, the pressure as a function of time is plotted for two selected points located at $(6.8, 0)$ and $(-0.8, 0)$ near the outflow and inflow boundaries respectively. The solid line is the numerical solution and circles represent a reference solution obtained by using a larger computational domain so that it is not affected by any boundary effects. Excellent agreement is found between the numerical and reference

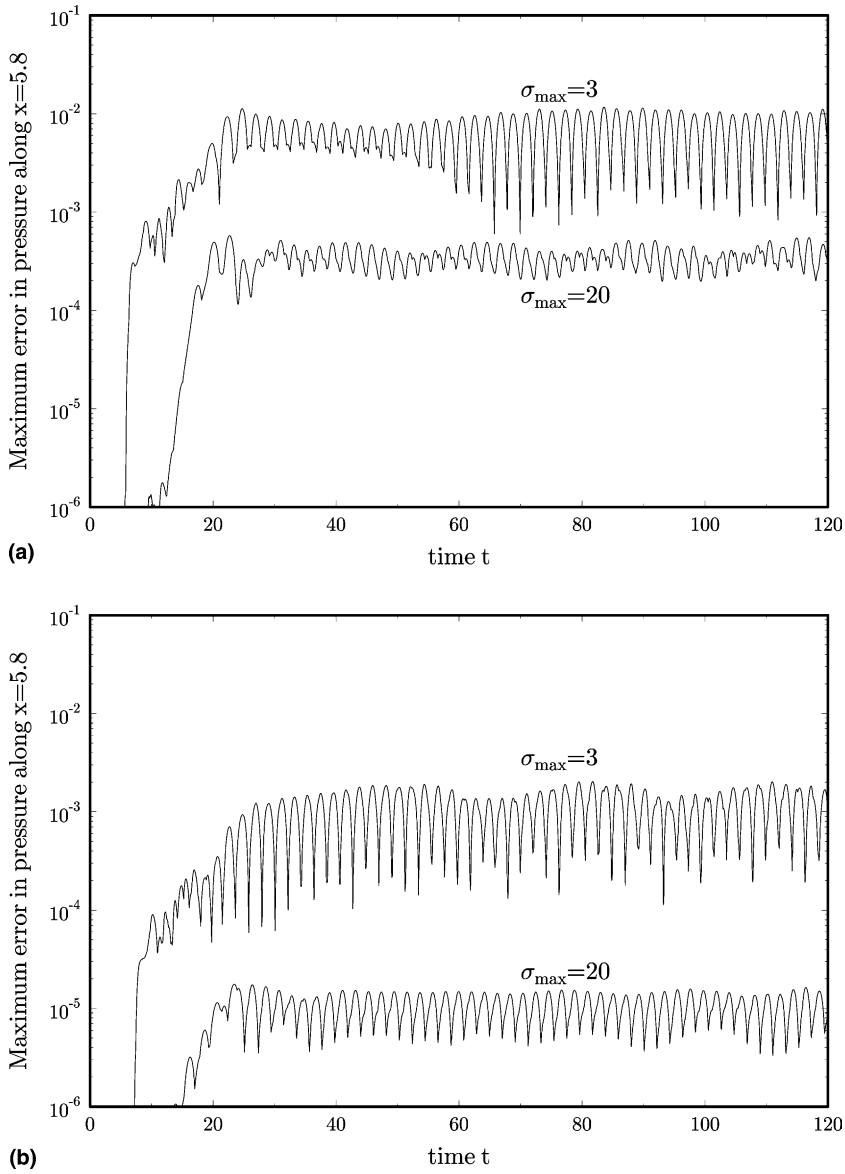

Fig. 11. Maximum difference between the numerical and reference solutions along $x = 6.8$ as a function of time: (a) $D = 10\Delta x$; (b) $D = 20\Delta x$.

solutions with no discernible difference on the graphic scale. For a quantitative measure of the reflection error, the maximum difference between the numerical and reference solutions on all grid points along $x = 6.8$ near the exit boundary is plotted in Fig. 11. The top graph shows the results using 10 grid points in the PML zone and the bottom graph using 20 points, with two cases of $\sigma_{max} = 3$ and 20 in each graph. Obviously, more absorption is achieved when a larger value of σ_{max} is used. Since the amplitude of the Kelvin–Helmholtz wave at the exit is about 0.1, Fig. 11 indicates that the reflection error is less than 1%

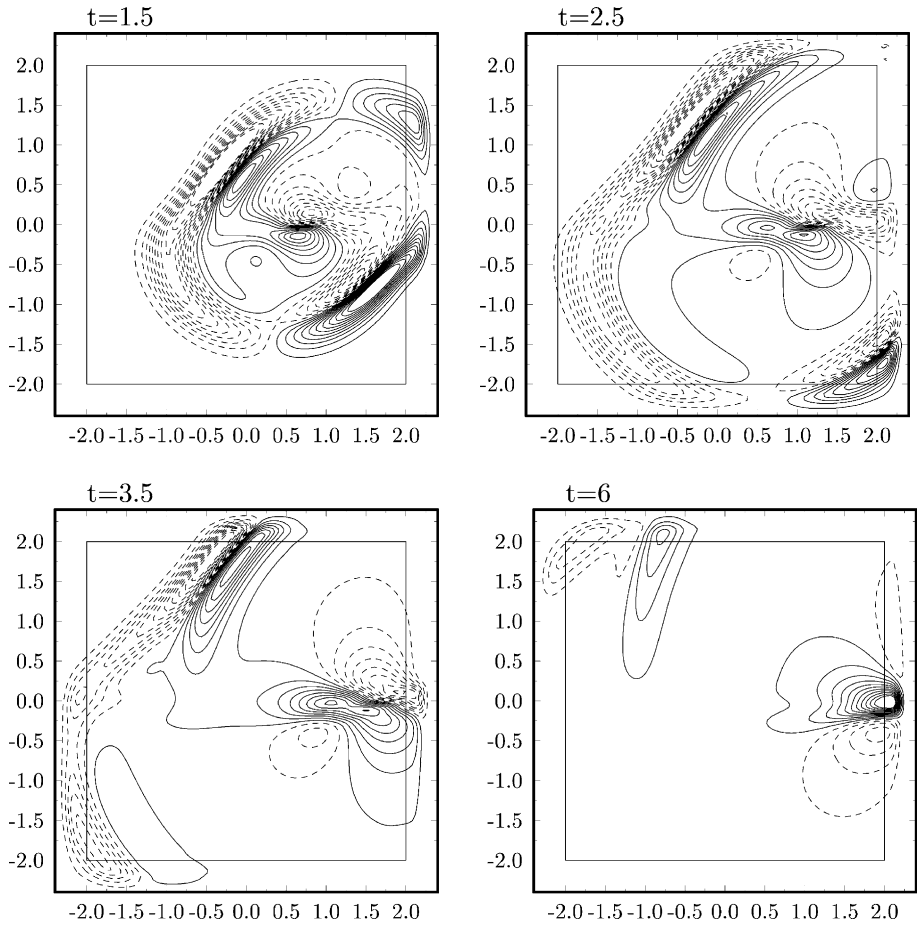

Fig. 12. u-Velocity contours, at the time as indicated.

when 10 grid points are used in the PML domain and the reflection is less than 0.1% with 20 grid points and $\sigma_{\max}$ being 20.

We note that even when the maximum value of the absorption coefficient $\sigma_{\max}$ used in this example is greater than the stability limiting value σ_s, which is 3 for the current mean flow, no numerical instability has been observed in the computation. This suggests that grid stretching combined with numerical filtering may be sufficient to suppress the growing modes identified in Fig. 7(c) when σ_x is beyond the stability limiting value σ_s.

7.2. Unbounded mixing layer

In the second example, the propagation of an acoustic pulse in an unbounded shear flow, specified again by (14) and (15), is simulated. The computational domain is $[-2.4, 2.4] \times [-2.4, 2.4]$ with PML zones, consisting of 10 grid points, on all four sides. Eq. (37), without the $\mathbf{q}'$ term, is used for the PML zones. The value of $\beta = -1/c_0$ where $c_0 = -1.416$ is obtained by assuming that the flow is bounded at $y = \pm 2.4$, which is only slightly different from that found in the previous example. The initial condition is

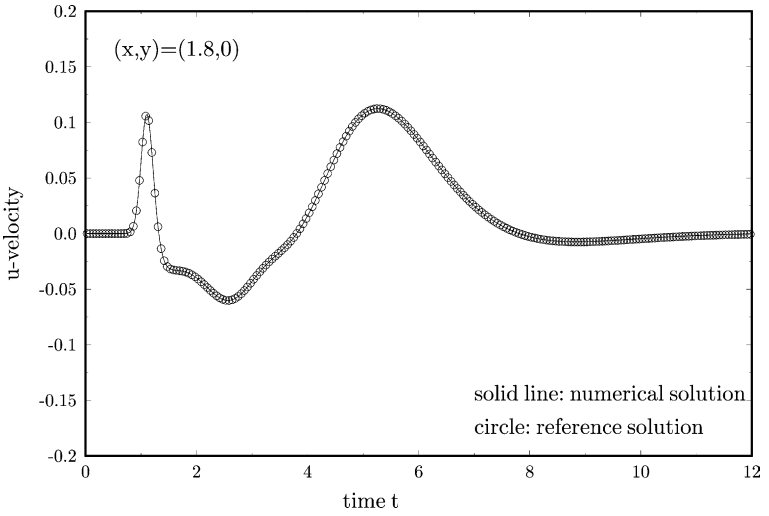

Fig. 13. u-Velocity time history at point $(x, y) = (1.8, 0)$. Solid line: numerical solution; circles: reference solution.

$$t = 0, \quad u = v = \rho = 0, \quad p = \mathrm{e}^{-(\ln 2)(x^2+y^2)/0.2^2}.$$

Fig. 12 shows the u-velocity contours at $t = 1.5$, 2.5, 3.5 and 6. The initial acoustic pulse as well as the vorticity wave induced by the shear flow are absorbed effectively at the boundaries. Fig. 13 shows the time history of the u-velocity at a sample point (1.8, 0) near the outflow boundary. The numerical (solid line) and reference (circles) solutions are again in excellent agreement. The maximum difference between the numerical and reference solutions for the pressure along $x = 1.8$ is plotted in Fig. 14, which shows that the use of PML caused little reflection.

7.3. Unbounded jet flow

In the third example, the acoustic radiation of a point source located inside a subsonic jet is simulated. The jet mean velocity and density are given by

$$\bar{u} = U_a + (U_j - U_a)\mathrm{e}^{-(\ln 2)y^2/0.3^2}, \quad \bar{\rho} = 1, \tag{42}$$

where $U_a = 0.2$ and $U_j = 0.5$. A source term of the form

$$s(x, y, t) = \sin(20\pi t)\mathrm{e}^{-(\ln 2)[(x+0.5)^2+y^2]/0.03^2}$$

is added to the equation for the pressure. The computational domain is $[-1.1, 1.1]\times[-1.1, 1.1]$, with $\Delta x = \Delta y = 0.01$. The PML domains on all four sides have a width of 10 grid points.

For the mean flow given in (42), the spectral collocation method for the linear wave analysis suggests a value of 0.3124 for β. Formula (28), given for a constant mean density, yields the same value for β as well.

Fig. 15 plots instantaneous pressure contours and shows clean absorption of out-going waves. The mean flow refraction effect is also notable. At the current high frequency for the source, the jet instability wave is not excited. To compare with a reference solution, the pressure history at a sample point $(x, y) = (0.95, 0.5)$ near the outflow boundary is plotted in Fig. 16. Again we see excellent agreements.

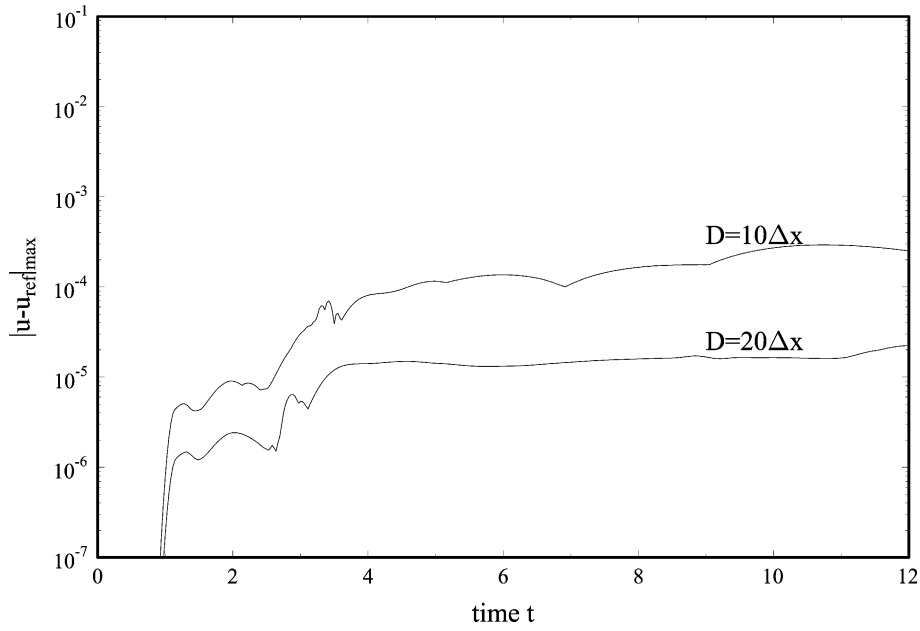

Fig. 14. Maximum difference between the numerical and reference solutions along $x = 1.8$ as a function of time.

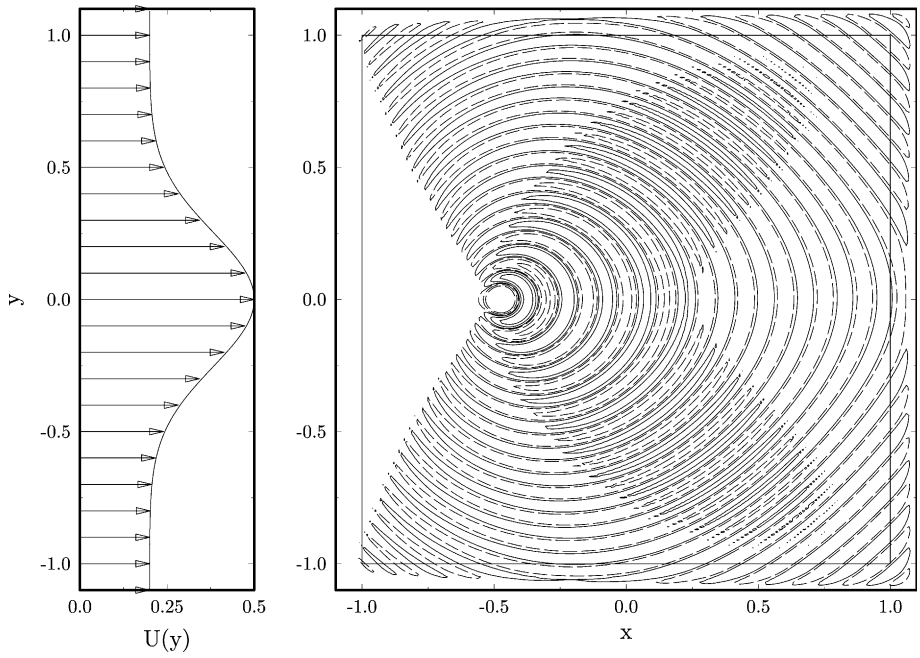

Fig. 15. Instantaneous pressure contours (right) and the mean velocity profile (left).

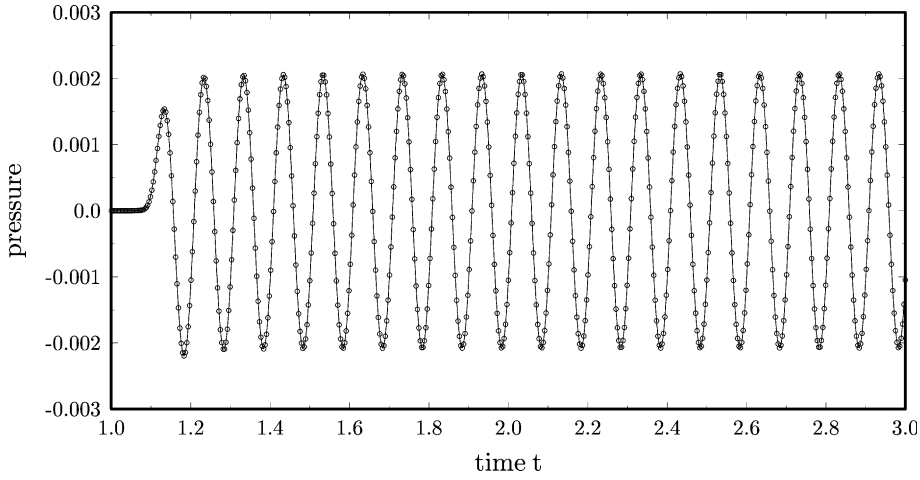

Fig. 16. Pressure history at point $(x, y) = (0.95, 0.5)$. Solid line: numerical solution; circles: reference solution.

8. Conclusions

A Perfectly Matched Layer is presented as an absorbing boundary condition for the linearized Euler equations with a parallel non-uniform mean flow. It applies to both bounded (ducted) and unbounded flows. It is shown that for the stability of PML it is of critical importance to apply a proper space–time transformation in the derivation of PML equation. The parameter for the proper space–time transformation can be determined a priori from the dispersion relations of acoustic modes supported by the mean flow. Numerical examples show that the PML formulated here works well for subsonic compressible shear flows.

It is further shown that the proposed PML is dynamically stable for a finite range of the absorption coefficient. Since the precise stability limit on the absorption coefficient is very much mean flow dependent and can only be obtained through a stability analysis of the PML equations for the specific mean flow profile, it is recommended that certain numerical dissipation be introduced in the PML domain, such as numerical filtering or numerical damping. In all the computational examples reported here, a use of high order numerical filtering and grid stretching has been sufficient for suppressing the non-physical unstable modes when the absorption coefficient is moderately greater than the stability limiting value.

Acknowledgement

This work is supported in part by a grant from NASA Langley Research Center NAG1-03037 and by a grant from the National Science Foundation DMS-0411402. The author also would like to thank the reviewers for their constructive comments.

Appendix A. Spectral collocation method

In this appendix, we describe the spectral collocation method used to solve the eigenvalue problem posed by (12) and (13). Assuming that the computational domain for y is $[-1, 1]$, we expand the solution $\hat{\mathbf{u}}(y)$ in basis polynomials as follows:

$$\hat{\mathbf{u}}(y) = \sum_{n=0}^{N} \begin{pmatrix} \rho_n \phi_n(y) \\ u_n \phi_n(y) \\ v_n \psi_n(y) \\ p_n \phi_n(y) \end{pmatrix}, \tag{A.1}$$

where $\{\phi_n\}$ and $\{\psi_n\}$ are formed by the Chebychev polynomials $T_n(y)$ as

$$\psi_n(y) = \begin{cases} T_0(y) - T_{n+2}(y), & n \text{ even}, \\ T_1(y) - T_{n+2}(y), & n \text{ odd}, \end{cases}$$

$$\phi_n(y) = \begin{cases} 1, & n = 0, \\ \left(\frac{n+2}{2}\right)^2 T_2(y) - T_{n+2}(y), & n \text{ even}, \\ (n+2)^2 T_1(y) - T_{n+2}(y), & n \text{ odd}. \end{cases}$$

The expansion (A.1) automatically satisfies the boundary condition for $\hat{\mathbf{u}}(y)$ [22]. By substituting (A.1) into (12) and requiring that the equation be satisfied at collocation points,

$$y_j = \cos\left(\frac{2j+1}{2N+2}\pi\right), \quad j = 0, 1, 2, \ldots, N,$$

we get

$$\sum_{n=0}^{N} \left[-\mathrm{i}\omega \begin{pmatrix} \rho_n \phi_n \\ u_n \phi_n \\ v_n \psi_n \\ p_n \phi_n \end{pmatrix} + \mathrm{i}k\mathbf{A} \begin{pmatrix} \rho_n \phi_n \\ u_n \phi_n \\ v_n \psi_n \\ p_n \phi_n \end{pmatrix} + \mathbf{B} \begin{pmatrix} \rho_n \phi_n' \\ u_n \phi_n' \\ v_n \psi_n' \\ p_n \phi_n' \end{pmatrix} + \mathbf{C} \begin{pmatrix} \rho_n \phi_n \\ u_n \phi_n \\ v_n \psi_n \\ p_n \phi_n \end{pmatrix} \right]_{y=y_j} = 0$$

for $j = 0, 1, 2, \ldots, N$. This can be easily cast into a generalized algebraic eigenvalue problem for ω of the form $\mathbb{Q}\vec{\mathbf{u}} = \omega\mathbb{R}\vec{\mathbf{u}}$ where $\vec{\mathbf{u}}$ is a vector consisting of all the expansion coefficients in (A.1) and $\mathbb{Q}$ and $\mathbb{R}$ are $(4N + 4) \times (4N + 4)$ matrices. For the results given in Fig. 3, $N = 63$.

References

[1] S. Abarbanel, D. Gottlieb, J.S. Hesthaven, Well-posed perfectly matched layers for advective acoustics, J. Comput. Phys. 154 (1999) 266–283.

[2] S. Abarbanel, D. Stanescu, M.Y. Hussaini, Unsplit variable perfectly matched layers for the shallow water equation with coriolis forces, Comput. Geosci. 7 (4) (2003) 265–294.

[3] E. Becache, A.-S. Bonnet-Ben Dhia, G. Legendre, Perfectly matched layers for the convected Helmholtz equations, SIAM J. Numer. Anal. 42 (1) (2004) 409–433.

[4] E. Becache, P.G. Petropoulos, S.D. Gedney, On the long-time behaviour of unsplit Perfectly Matched Layers, INRIA Report, No. 4538, 2002.

[5] E. Becache, S. Fauqueux, P. Joly, Stability of perfectly matched layers, group velocities and anisotropic waves, J. Comput. Phys. 188 (2003) 399–433.

[6] J.P. Berenger, A Perfectly Matched Layer for the Absorption of Electromagnetic waves, J. Comput. Phys. 114 (1994) 185–200.

[7] W.C. Chew, W.H. Weedon, A 3D perfectly matched medium from modified Maxwell's equations with stretched coordinates, IEEE Microwave Opt. Technol. Lett. 7 (1994) 599–604.

[8] G. Chimonas, The extension of the Miles-Howard Theorem to compressible fluids, J. Fluid Mech. 43 (1970) 833–836.

[9] F. Collino, P. Monk, The perfectly matched layer in curvilinear coordinates, SIAM J. Sci. Comput. 19 (6) (1998) 2016.

[10] P.G. Drazin, W.H. Reid, Hydrodynamic Stability, Cambridge University Press, 1981.

[11] S.D. Gedney, An anisotropic perfectly matched layer-absorbing medium for the truncation of FDTD lattices, IEEE Trans. Antennas Propagat. 44 (1996) 1630.

[12] T. Hagstrom, I. Nazarov, Absorbing layers and radiation boundary conditions for jet flow simulations, AIAA paper 2002–2606, 2002.
[13] T. Hagstrom, I. Nazarov, Perfectly matched layers and radiation boundary conditions for shear flow calculations, AIAA paper 2003–3298, 2003.
[14] F.Q. Hu, A numerical study of wave propagation in a confined mixing layer by eigenfunction expansions, Phys. Fluids A 5 (6) (1993) 1420–1426.
[15] F.Q. Hu, The acoustic and instability waves of jets confined inside an acoustically lined rectangular duct, J. Sound Vib. 183 (1995) 841–856.
[16] F.Q. Hu, On absorbing boundary conditions of linearized Euler equations by a perfectly matched layer, J. Comput. Phys. 129 (1996) 201–219.
[17] F.Q. Hu, On Perfectly Matched Layer as an absorbing boundary condition, AIAA paper 96–1664, 1996.
[18] F.Q. Hu, A stable, Perfectly Matched Layer for linearized Euler equations in unsplit physical variables, J. Comput. Phys. 173 (2001) 455–480.
[19] F.Q. Hu, Absorbing boundary conditions, Int. J. Comput. Fluid Dynamics. 18 (6) (2004) 513–522.
[20] F.Q. Hu, Solution of aeroacoustics benchmark problems by discontinuous Galerkin method and Perfectly Matched Layer for nonuniform mean flows, in: Proceeding of the 4th CAA Workshop on Benchmark Problems, NASA CP-2004-212954 (2004) 335–353.
[21] F.Q. Hu, M.Y. Hussaini, J.L. Manthey, Low dissipation and low dispersion Runge–Kutta schemes for computational acoustics, J. Comput. Phys. 124 (1996) 177–191.
[22] F.Q. Hu, C.K.W. Tam, Parametric instability of supersonic shear layers induced by periodic Mach wave, Phys. Fluids A 6 (3) (1991) 1645–1656.
[23] H. Huerre, P.A. Monkewitz, Local and global instabilities in spatially developing flows, Annu. Rev. Fluid Mech. 22 (1990) 473.
[24] L.M. Mack, On the inviscid acoustic-mode instability of supersonic shear flows, Theor. Comput. Fluid Dynamics 2 (1990) 97–123.
[25] S.A. Orszag, Accurate solution of the Orr-Sommerfeld stability equation, J. Fluid Dynamics 50 (1971) 689–703.
[26] P.G. Petropoulos, Reflectionless sponge layers as absorbing boundary conditions for the numerical solution of Maxwell's equations in rectangular, cylindrical and spherical coordinates, SIAM J. Appl. Math. 60 (2000) 1037–1058.
[27] C.K.W. Tam, L. Auriault, F. Cambulli, Perfectly Matched Layer as an absorbing boundary condition for the linearized Euler equations in open and ducted domains, J. Comput. Phys. 144 (1998) 213–234.
[28] C.K.W. Tam, F.Q. Hu, On the three families of instability waves of high-speed jets, J. Fluid Mech. 201 (1989) 447–483.
[29] C.K.W. Tam, F.Q. Hu, Acoustic and instability waves of a confined supersonic mixing layer, J. Fluid Mech. 203 (1989) 51–76.
[30] C.K.W. Tam, J.C. Webb, Dispersion-relation-preserving finite difference schemes for computational acoustics, J. Comput. Phys. 107 (1993) 262–281.
[31] E. Turkel, A. Yefet, Absorbing PML boundary layers for wave-like equations, Appl. Numer. Math. 27 (1998) 533–557.
[32] G.B. Witham, Linear and Nonlinear Waves, Wiley, 1978.
[33] L. Zhao, A.C. Cangellaris, GT-PML: generalized theory of perfectly matched layers and its application to the reflectionless truncation of finite-difference time-domain grids, IEEE Trans. Microwave Theory Tech. 44 (1996) 2555–2563.
[34] M. Zhuang, Instability of wake-dominated compressible mixing layers, Phys. Fluids 7 (1995) 2489–2495.